Propagation of hot electrons through high-density plasmas

H. Teng,[1] J. Zhang,[1,*] Z. L. Chen,[1] Y. T. Li,[1] K. Li,[1] X. Y. Peng,[1] and J. X. Ma[2]
[1]*Laboratory of Optical Physics, Institute of Physics, Chinese Academy of Sciences, Beijing 100080, People's Republic of China*
[2]*Department of Modern Physics, University of Science and Technology, Anhui, People's Republic of China*
(Received 11 March 2002; revised manuscript received 3 December 2002; published 10 February 2003)

Propagation of hot electrons through high-density plasmas generated by femtosecond laser pulses is investigated using three types of target configurations: Al-coated glass, Al and glass separated by a vacuum gap, and Al foil alone. Collimated ionization tracks lasting for 60 ps and extending 150–300 μm in length and 8 μm in cross section are observed via optical probing. For the Al-foil-alone target, a narrow plasma jet is formed at the rear surface in line with the laser. The collimation of the hot electrons may be attributed to a strong self-generated magnetic field in the target.

DOI: 10.1103/PhysRevE.67.026408 PACS number(s): 52.50.Jm, 52.40.−w, 52.25.Os, 52.38.−r

I. INTRODUCTION

With the advent of multiterawatt short pulse lasers [1], the ''fast ignition'' scheme [2] was proposed, by which an intense short laser pulse is focused onto a high-density precompressed thermonuclear fuel to generate hot electrons and create an ignition spark that initiates a propagating thermonuclear burn. This separation of compression and ignition greatly reduces the driver energy and relaxes the symmetry requirements for the compression. There are still several technical challenges to the fast ignition scheme, e.g., ''hole boring'' of short pulse laser in the low-density plasma region [3], efficient penetration of the laser into the high-density region though self-channeling [4], and interaction of the laser with the high-density fuel core to generate copious relativistic electrons [5]. Ideally, the electrons should propagate as a stable beam into the compressed fuel and deposit their energy in a small volume and heat the fuel to fusion temperature locally. Thus, in fast ignition, one of the critical issues is the propagation of hot electrons through high-density plasmas.

Several mechanisms that can transfer laser energy to the plasma electrons have been proposed [6]. One is the ponderomotive acceleration, in which the $\mathbf{v}\times\mathbf{B}$ force ponderomotively accelerates the electrons in the direction of laser propagation [7,8]. Other mechanisms include collisionless electron acceleration at the critical density, such as vacuum heating [9,10], resonant absorption [11], and parametric instabilities [12]. In addition, magnetic and electric fields, variable resistivity, as well as collisions can all play important roles on the propagation of hot electrons in a dense plasma. The latter have been studied by many measurements, such as $K\alpha$ emission diagnostics [13], γ-ray spectra, two-dimensional (2D) transverse imaging of solid target with a probe beam [14–17], and direct imaging of the emission from the hot electrons [18].

In this paper, we present an experimental investigation on the propagation of hot electrons through high-density plasmas. A bundle of ionization tracks was observed via optical probing inside two types of Al-coated glass targets. In order to understand the behavior of the hot electrons right after their generation, the plasma jet at the rear surface of a 20 μm Al foil was also analyzed via optical probing. The acceleration and propagation of the electrons may be attributed to the ponderomotive force and their collimation to the self-generated magnetic field inside the target.

II. EXPERIMENTAL SETUP

The experiment is performed on the Ti:sapphire terawatt laser system ''JIGUANG-I'' [19] operating at 800 nm at a repetition rate of 10 Hz based on chirped pulse amplification. The system delivers up to 36 mJ energy in 25 fs, corresponding to a peak power of 1.4 TW. Low-energy equivalent-plane measurements show a 10–20 μm full width at half maximum focal spot, giving a maximum intensity of 1×10^{17} Wcm^{-2}. The targets used are 1-μm-aluminum-coated fused glass slide, 5-μm aluminum on fused glass slide with a vacuum gap, and 20-μm-thick aluminum foil only. The roughness of the surfaces is less than 1 μm. The mount is controlled by three-dimensional microstep motor, in order to ensure that the laser pulse interacts with a fresh target surface at each shot.

The experimental setup is shown in Fig. 1. The laser pulse

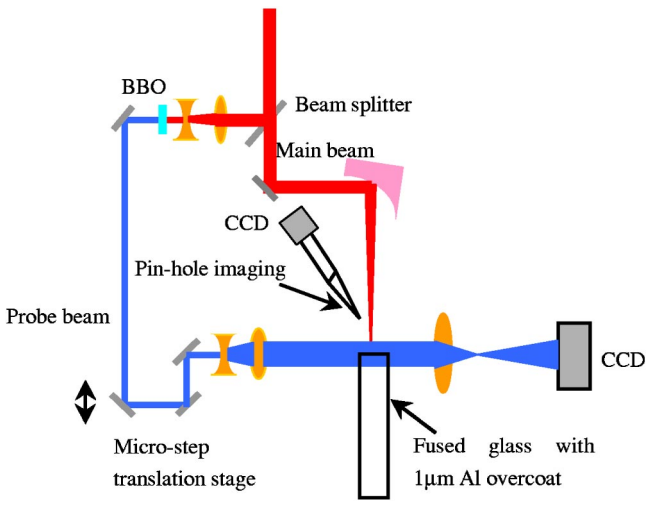

FIG. 1. Schematic of the experimental setup.

*Corresponding author. Email address: jzhang@aphy.iphy.ac.cn

is focused onto the target at 10° to the normal. A pinhole imaging of x-ray emission monitors the focal spot size for each full energy shot. A small fraction of the main beam, after frequency doubling to 400 nm in a BBO crystal, is used as a temporally independent probe beam. The latter passes transversely across the target. The front surface and target interior are in the field of view. A charge coupled device with a 400-nm band transmission filter is used to obtain a side view of the target at spatial and temporal resolutions of the order of 1 μm and 1 ps, respectively. A region that has been ionized up to a fraction of the critical density (of 400-nm light) becomes opaque to the probe. Refraction of the probe light in strong density gradients limits our observation to regions with electron density less than 6.9×10^{21} cm^{-3}. By varying the time delay between the probe and the main beam, we can analyze the ionized channels in the fused glass and the plasma at the rear surface of Al foil. The probe beam is timed by decreasing the relative delay to a value such that no plasma is seen. This value is taken to be the zero point of time.

A calibrated γ-ray spectrometer was also used to monitor the x-ray bremsstrahlung from the laser plasma. The γ-ray spectrometer consists of a NaI detector, an electronic gated shutter, a photomultiplier, an amplifier, and a multichannel energy analyzer. A 20-mm-diameter hole in a 50-mm-thick Pb block is used to collimate the x-ray radiation and to shield the detector. The detector response is calibrated using a 511-keV and 1.274-MeV γ-ray ^{22}Na source and a 665-keV ^{137}Cs source.

III. RESULTS AND DISCUSSION

The bremsstrahlung hard x-ray spectrum has the same Maxwellian distribution as the colliding electrons. The hard x-ray spectrum is generally dominated by the bremsstrahlung produced by the high-energy hot electrons colliding with atom nuclei. The shape and intensity of the bremsstrahlung is the principal diagnostic for the outgoing hot electron flux and temperature. The hard x-ray spectrum shows a bi-Maxwellian distribution and the hot electron temperature is 73 keV, as shown in Fig. 2. However, the space-charge field stops hot electrons with energies below $\sim$20 keV, so that the outgoing hot electron temperature is about 90 keV. The energy spectra of the outgoing and the incoming (to the glass) hot electrons are the same, hence the incoming hot electron temperature is also 90 keV. Propagation of these hot electrons through the high-density material is investigated below.

Shadowgrams of the target are recorded at different times. Figure 3 shows a typical shadowgram for the 1-μm-aluminum-coated fused glass slide at different times after the interaction. In order to enhance the contrast of this particular image, we have subtracted from it the image of the unperturbed target in the presence of the probe beam. Before the interaction, the fused glass slide is transparent to the probe beam. At the interaction, plasma formation can clearly be seen at the left edge of the Al-coated fused glass target. The dark region corresponds to a plasma density greater than 6.9×10^{21} cm^{-3} (the critical density of 400-nm light). It is also seen that the plasma expansion into the vacuum is not exactly cone shaped. This shows that the evolution from

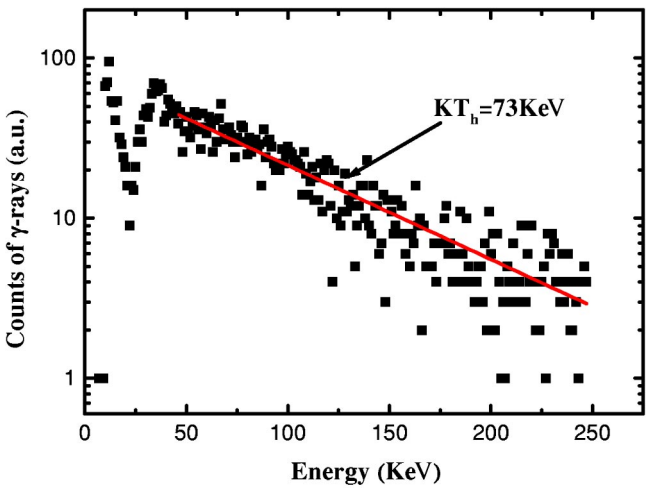

FIG. 2. The bremsstrahlung x-ray radiation from the Al target. The solid line in the figure is the Maxwellian distribution fit for the temperature.

compression to expansion of the plasma is due to the laser ponderomotive force. Opposite to the direction of the plasma expansion, a nearly isotropic dark region can clearly be seen. In view of the velocity ($\sim2\times10^8$ cm/s) of the expansion, the almost isotropic dark region may be attributed to radiation driven thermal transport ionization waves [20]. Furthermore, a few narrow jets above the ionization wave, originating from the interaction region, can be seen. In some images, there are many narrow jets, parallel to each other, with similar size (8-μm cross section, 150–300 μm long) and separation distance (13 μm). These jets in the transparent glass slide are opaque to the probe beam, suggesting that they are dense plasma tracks corresponding to local ionization in the glass.

Three mechanisms can induce the ionization tracks in the glass: laser light, hard x rays, and hot electrons. During the interaction, the laser itself may penetrate into and form filaments within the target. However, the 1-μm-thick Al coating on the glass should block the incident laser. The contrast ratio of the laser pulse is 10^5 at 1 ps (measured by a high-dynamic third autocorrelator). A particle-in-cell simulation (Figs. 4 and 5) shows that the prepulse at 1 ps does not ablate the 1-μm Al, and only after 100 ps a shock wave propagates through the 1-μm Al. On the other hand, prior to that hot electrons produced in the interaction propagate through and out of the Al foil. Therefore, we can rule out the presence of laser light filaments in the glass. Furthermore, the cross section of the target surface was 1 mm, so that there is no possibility that light from the outer part of the laser pulse could wrap around the side of the target and initiate ionization.

Besides the hot electron beams, strong x-ray bremsstrahlung and thermal emission generated by the interaction may also propagate into the target and cause ionization tracks. In order to rule out the latter possibilities, a series of shots on a composite target were performed. The composite target consists of a vacuum gap between a 5-μm Al foil and fused glass. For comparison, some shots are also performed on 20-μm aluminum-foil-only targets.

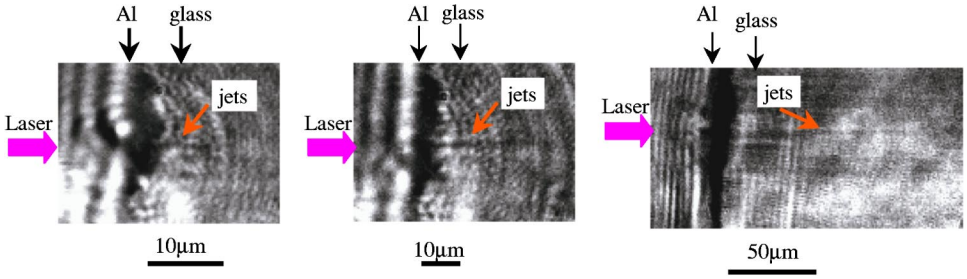

FIG. 3. Shadowgrams taken during the interaction of a 36-mJ, 25-fs laser with the 1-μm-Al-coated fused silica targets at three times: (a) 1 ps, (b) 3 ps, (c) 11 ps after the interaction. Note in pictures that the fringes at left of targets are diffraction patterns at the edge of targets.

When the laser pulse hits the Al-glass target with a vacuum gap, it first interacts with the Al foil. The regions of hot electron generation in the foil and transport through the glass are thus separated by a vacuum. A space-charge separation field builds up in the vacuum gap when the hot electrons move across it. Figure 6 shows a shadowgram taken at 13 ps after the interaction. Formation of the space-charge induced plasma in the vacuum gap at the rear surface of Al foil can be observed together with the jets in the glass slide. However, the length of the jets in Fig. 6 is significantly shorter than that in Fig. 3. When the hot electrons exit the Al foil, the space charge separation field is about 10^{11} V m^{-1} [13,21], which will stop electrons with energies below 23 keV (assuming that sheath width is of the order of the Debye length). Hot electrons above 23 keV can still go through the space-charge plasma but with somewhat reduced energy, enter the glass, and induce ionization. Thus, the length of the jets is shorter, as can be seen in Fig. 6. This supports the assertion that the ionization tracks in the glass are caused by the high-energy electrons, since the length of jets would be the same if the ionization were caused by hard x rays. We can thus exclude the possibility of hard x-ray induced ionization in the glass.

We have also performed a series of shots on 20-μm Al foils without the glass backing. Figure 7 shows the shadowgram taken at the same time (13 ps) as in Fig. 6. We can clearly see a dark mushroomlike structure with a diameter of 10 μm at the rear surface of the Al foil. It is always in line with the laser focal spot and expands with time. The dark cone does not appear when there is only the main beam (no probe beam). Hence, the cone does not show self-emission, but emission from the plasma at the rear surface. The plasma formation at the rear surface could not be due to the laser light or hard x rays, since the laser is blocked by the 20-μm Al foil and hard x rays (that can penetrate the Al foil) do not form plasmas in vacuum. Moreover, from the formation time, we can also rule out shock breakout, which would induce a plasma cloud with much larger diameter. In addition, fast ions can also be ruled out because they cannot pass through thick targets. Therefore, hot electrons are the only source to produce the rear plasma. In our case, the average temperature of the hot electrons is about 93 keV, and their spatial range in aluminum is 62 μm. This is much longer than the thickness of the Al foil. Thus, the fast electrons, originated from the interaction area, can penetrate through the solid target. As they leave the rear surface, a space-charge field is set up, forming an electron sheath with a thickness of the order of the Debye length. If assuming the absorption into the hot electron is about 20% with a mean energy of 93 keV, and the hot electrons fill the 20-μm-thick target with a 45° cone angle, we find that the Debye length is 1.23×10^{-7} m. The electric field (from the expression $eE\lambda_D \approx kT$ [21]) in the sheath is about 7.6×10^{11} V/m, which is much higher than the field needed to cause ionization in aluminum. Hence, these fast electrons can heat the target and form a plasma on the rear surface of the foil. This feature demonstrates that the formation of plasma on the rear surface can only be due to the hot electrons. We have also varied the delay time of the probe beam. The time from generation of the plasma on the rear Al surface to its disap-

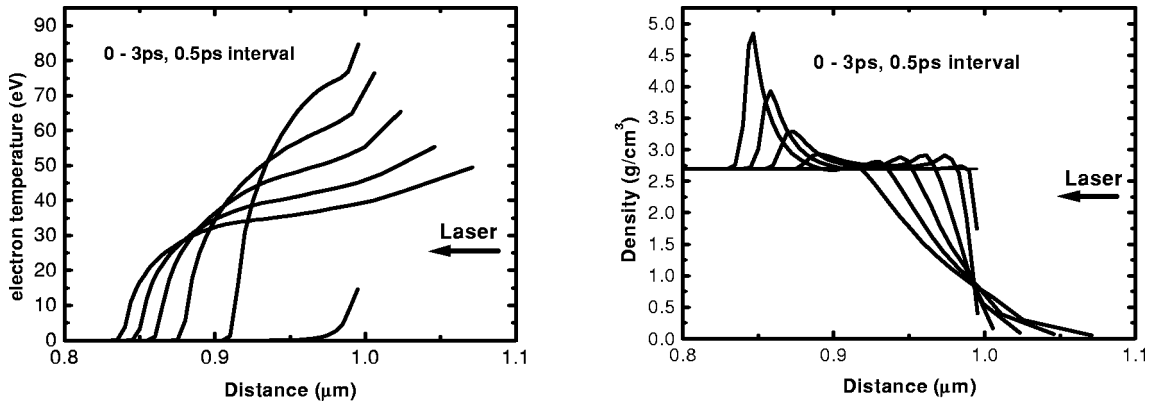

FIG. 4. Distribution of electron temperature and density for the 1-ps prepulse.

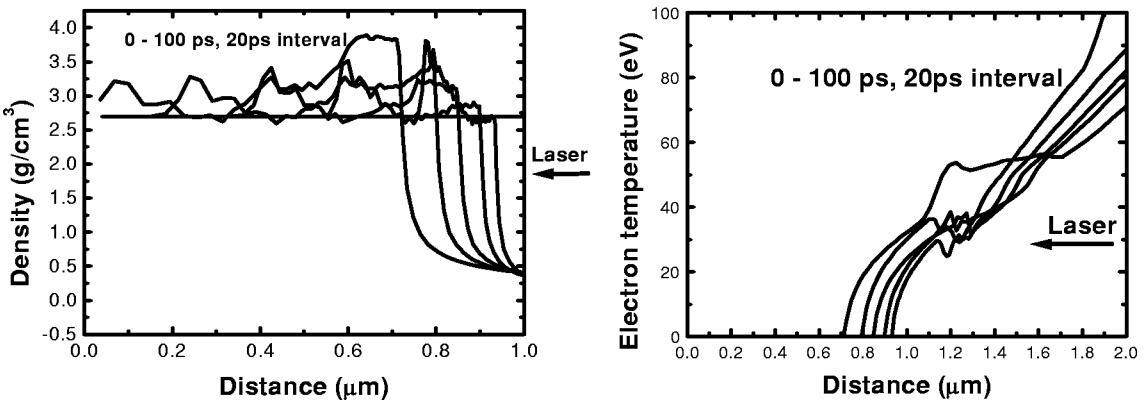

FIG. 5. Spatial distributon of electron temperature and density for the 100-ps prepulse.

pearance is about 60 ps, which is the same as the lifetime of the jets in the glass targets.

We propose that the jets in the transparent region are localized ionization region of hot electrons propagating through the glass. These hot electrons are generated in the interaction region, collimated by a strong magnetic field inside the target. The average hot electron energy can be obtained by many means, such as $K\alpha$ spectra, γ spectra, and fast electron spectra, etc. Using the results of Ref. [22] obtained from Kα emission measurements of laser solid experiments, the fast electron temperature is

$$kT_e \simeq 100\left(\frac{I\lambda^2}{10^{17}\ \mathrm{Wcm}^{-2}}\right)^{1/3}\ \mathrm{keV}, \tag{1}$$

where I and λ are the intensity and wavelength of the laser, respectively. The laser intensity is about 8×10^{16} W/cm^2, corresponding to an average hot electron energy of about 93 keV. From the table of energy losses and ranges of electrons and positrons [23], we find that the range is 110 μm for the 93-keV hot electrons in the glass. This is shorter than the length of jets observed. The discrepancy may be due to the existence of strong magnetic fields, which enhances the penetration of the hot electrons and reduces their angular spread [14]. Magnetic fields, electric fields, and plasma resistivity can all play important roles on hot electron transport. The ratio of the magnetic to electric force on the hot electrons is [24]

$$\frac{vB}{E} \simeq 12\left(\frac{2\tau}{1\ \mathrm{ps}}\right)\left(\frac{10\ \mu\mathrm{m}}{R}\right)\left(\frac{v}{c}\right), \tag{2}$$

where R is the focal spot size, τ is the duration of the laser pulse, and v is the hot electron speed. Thus, the effect of the magnetic field is significant. Simulation [21,24] has also shown that the electric field is not a major effect at an intensity of 10^{16} Wcm^{-2}. In the present case, the fast electrons are pinched inside the target by a strong magnetic field. Figure 6 shows that the diameter of the plasma at the rear surface of the Al foil is small, corresponding to a spreading angle of 10° over 20 μm. This is comparable to the radius of the observed plasma. If the fast electrons had propagated freely, the spread angle would be greater than 32° in the 20-μm foil target due to collisional scattering of electrons with atom nuclei. Strong magnetic fields [25] that are ubiquitous to the interaction of intense lasers with high-density plasmas can suppress the radial spread of the hot electron.

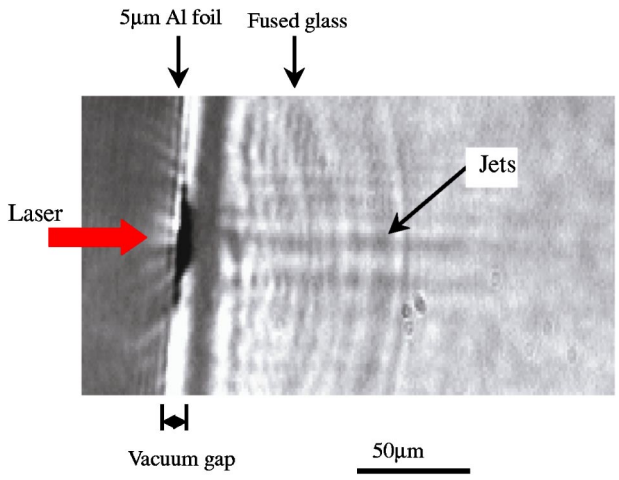

FIG. 6. Shadowgraphic image of the target during interaction of the main pulse with a composite target comprising a vacuum gap.

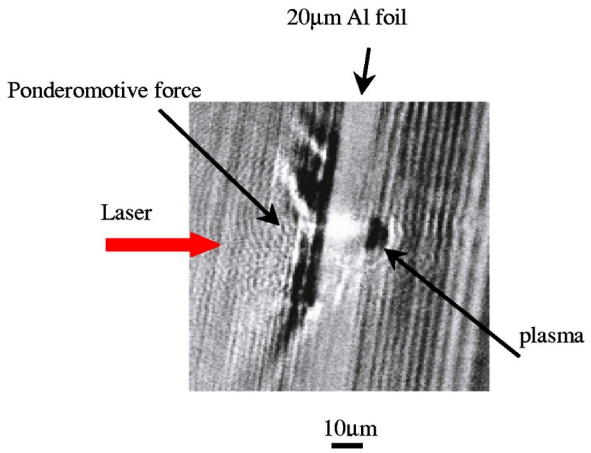

FIG. 7. Shadowgram taken during the interaction of 36-mJ, 25-fs laser with a 20-μm Al foil, showing a plasma on the rear surface.

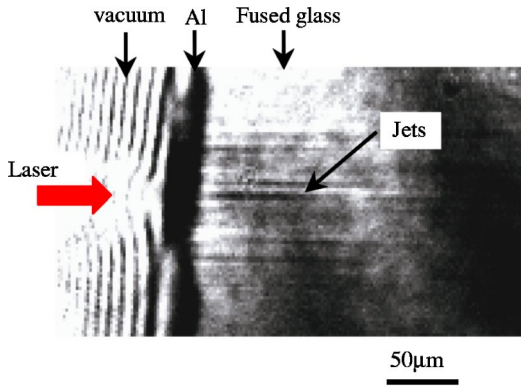

FIG. 8. Shadowgram taken during the interaction of the 36-mJ, 25-fs laser with a 1-μm-Al-coated fused glass. There are many more jets that are parallel to each other and their extension is wider than the focal spot.

The well collimated fast electrons give indirect evidence for the presence of such a magnetic field in the target.

It is of interest to note that in Fig. 8 there are two jets at the center of the focal spot, and several jets parallel but away from the axis of laser. This phenomenon is due to two reasons. The first is the fact that the focal spot was determined by low-energy equivalent-plane measurements, which showed a full width at half maximum of 10–20 μm. When energy is increased, the laser beam quality is strongly modulated by thermal effects and inhomogeneity of the dope concentration in the Ti:sapphire crystal. Thus there exist hot spots in the laser beam. When the laser is focused, there are many small local high intensity spots around the focus. Thus the effective size of the focal spot is much larger than that measured by low-energy equivalent-plane measurements. The intensity of each hot spot in the laser beam is sufficiently high to produce hot electrons to induce ionization in the fused silica. Thus the jets induced by the hot electrons can extend far from the axis of laser. This also explains why the length of jets was also almost the same, since the energy of each hot spot is almost the same. The second reason is due to Weibel instability [26], the measured beam size is full width at half maximum, because the hot electron beam is a Gaussian distribution, in fact, there are still some electrons near the bottom of the Gaussian distribution. When filaments were produced due to the splitting of the hot electrons, some hot electrons are diffused to two sides and the size of distribution becomes larger. Thus the jets induced by the hot electrons can extend far from the axis of the laser due to Weibel instability too.

Inside the target, the hot electron jets are parallel to the laser axis and they ionize the medium to form a bundle of parallel ionized filaments of dense plasma. The structure of the jets in the transparent targets is consistent with the results of the 2D simulation [27,28]. The filaments are the result of the splitting of the hot electron beam due to the Weibel instability [26,29], which generates strong magnetic fields transverse to the propagation direction of the hot electron beam, and the magnetic field in turn causes the beam to break up. The duration of the jets inside the target is 60 ps, which is longer than that from other observations [17]. The ionization and recombination time is very short in the dense plasma of the filaments, so that an accurate measure of the duration is difficult. Furthermore, the resistive and dielectric properties of the plasma, as well as the electric and magnetic fields, play important roles in determining the duration of the jets. As a rough estimate, the duration can be calculated from the characteristic time of collisions between the electrons and ions [30],

$$\tau_{ei} \simeq 3.5 \times 10^8 A T_e^{1.5} / N_0 Z_{av}^2, \tag{3}$$

where $A=20$ is the atomic mass number of the ions, T_e is the electron temperature in the unit of eV, N_0 is the plasma density, Z_{av} is the average charge number of the ions. For the parameters of our experiment we obtain $\tau_{ei} \simeq 22$ ps. Since the collision frequency of charge particles in the presence of magnetic field is smaller than that without the latter [31–33], the characteristic time of the jets will be longer when a strong magnetic field is present. Thus the duration of the jets in the experiment is in reasonable agreement with the estimate.

The conversion efficiency of laser energy into that of the hot electrons can be estimated from the structure of the closely packed bundle of ionized filaments in the glass. From the total ionized filament volume and the ionization energy of fused silica, the number of hot electrons can be estimated to be about 10^{11}. Thus, the conversion efficiency of laser energy into hot electrons is about 8%. This can also be obtained from the energy balance equation $n_e \varepsilon_e v_e = \eta I$, where n_e is electron density, ε_e is electron kinetic energy, η is the efficiency of laser energy conversion into hot electrons, and v_e is the velocity of hot electrons. For the intensity in our case, it is estimated that η is in the range of a few to ten percent. This is in accordance with the above estimate as well as with some other measurements [34].

IV. CONCLUSION

In conclusion, the propagation of hot electrons through high-density plasmas has been studied using optical probing techniques. A number of ionization tracks produced by hot electrons have been observed inside Al-coated glass targets. The plasma on the rear surface of a 20-μm Al foil has also been analyzed via optical probing. The jetlike tracks in the Al-coated fused glass originate from the focal spot, with about 150–300 μm in length and 8 μm in width. These tracks are parallel to each other and separated by a distance of 13 μm. The jets have a transverse structure and form bundles of ionized filaments. The structure is consistent with 2D PIC simulation, which shows that the propagation of a beam of hot electrons generated in the interaction region and propagates through the target is highly collimated by a strong self-generated magnetic field in the target.

ACKNOWLEDGMENTS

This work was jointly supported by the NNSFC (under Grant Nos. 10075075, 10005014, and 19825110), the National Hi-tech ICF program, and the NKBRSF (under Grant No. G19999075200).

[1] P. Maine *et al.*, IEEE J. Quantum Electron. **24**, 398 (1998).
[2] M. Tabak *et al.*, Phys. Plasmas **1**, 1626 (1994).
[3] R. Krushelnick *et al.*, Phys. Rev. Lett. **78**, 4047 (1997).
[4] M. Borghesi *et al.*, Phys. Rev. E **57**, 4899 (1998).
[5] C. Deutsch *et al.*, Phys. Rev. Lett. **70**, 3075 (1993).
[6] S.C. Wilks and W.L. Kruer, IEEE J. Quantum Electron. **33**, 1954 (1997).
[7] W. Yu *et al.*, Phys. Rev. E **61**, 2220 (2000); Y.T. Li *et al.*, *ibid.* **64**, 046407 (2001).
[8] S.C. Wilks *et al.*, Phys. Rev. Lett. **45**, 1383 (1992).
[9] F. Brunel, Phys. Rev. Lett. **59**, 52 (1987).
[10] L.M. Chen, J. Zhang *et al.*, Phys. Plasmas **8**, 2925 (2001); Q.L. Dong and J. Zhang, *ibid.* **8**, 1025 (2001).
[11] N.H. Ebrahim *et al.*, Phys. Rev. Lett. **45**, 1179 (1980).
[12] K. Estabrook and W.L. Kruer, Phys. Fluids **26**, 7 (1983).
[13] M. H. Key *et al.*, Phys. Plasmas **5**, 1966 (1998).
[14] M. Tatarakis *et al.*, Phys. Rev. Lett. **81**, 999 (1998).
[15] T.A. Hall *et al.*, Phys. Rev. Lett. **81**, 1003 (1998).
[16] D. Batani *et al.*, Phys. Rev. E **61**, 5725 (2000).
[17] M. Borghesi *et al.*, Phys. Rev. Lett. **83**, 4309 (1999); L. Gremillet *et al.*, *ibid.* **83**, 5015 (1999).
[18] R. Kodama *et al.*, Nature (London) **412**, 798 (2001).
[19] Z.Y. Wei *et al.*, Sci. China, Ser. A: Math., Phys., Astron. **43**, 1083 (2000).
[20] T. Ditmire *et al.*, Phys. Rev. Lett. **77**, 498 (1996).
[21] J.R. Davies *et al.*, Phys. Rev. E **59**, 6032 (1999).
[22] F.N. Beg *et al.*, Phys. Plasmas **4**, 447 (1996).
[23] M. J. Berger and S. M. Seltzer, *Studies in Penetration of Charged Particles in Matter* (National Academy of Sciences, Washington, D.C., 1964).
[24] J.R. Davies *et al.*, Phys. Rev. E **56**, 7193 (1997).
[25] J. Stamper, Science **281**, 1469 (1998).
[26] T. Taguchi *et al.*, Phys. Rev. Lett. **86**, 5055 (2001).
[27] A. Pukhov and J. Meyer-ter-Vehn, Phys. Rev. Lett. **79**, 2686 (1997).
[28] A. Pukhov, Phys. Rev. Lett. **86**, 3562 (2001).
[29] R.L. Morse and C.W. Nielson, Phys. Fluids **14**, 830 (1971); T. Yabe and K. Mima *et al.*, Phys. Rev. Lett. **48**, 242 (1982); T. Taguchi *et al.*, *ibid.* **86**, 5055 (2001).
[30] L. Spitzer, *Physics of Fully Ionized Gases* (Wiley, New York, 1962).
[31] S. Imazu, Plasma Phys. Controlled Fusion **28**, 857 (1986).
[32] S. Imazu, Phys. Rev. A **23**, 2644 (1981).
[33] D. Montgomery, Phys. Fluids **17**, 2201 (1974).
[34] J. Yu *et al.*, Phys. Plasmas **6**, 1318 (1999).